

Optimal Error Correction in Topological Subsystem Codes

Ruben S. Andrist,¹ H. Bombin,² Helmut G. Katzgraber,^{3,1} and M. A. Martin-Delgado⁴

¹*Theoretische Physik, ETH Zurich, CH-8093 Zurich, Switzerland*

²*Perimeter Institute for Theoretical Physics, Waterloo, Ontario N2L 2Y5, Canada*

³*Department of Physics and Astronomy, Texas A&M University, College Station, Texas 77843-4242, USA*

⁴*Departamento de Física Teórica I, Universidad Complutense, 28040 Madrid, Spain*

(Dated: March 2, 2013)

A promising approach to overcome decoherence in quantum computing schemes is to perform active quantum error correction using topology. Topological subsystem codes incorporate both the benefits of topological and subsystem codes, allowing for error syndrome recovery with only 2-local measurements in a two-dimensional array of qubits. We study the error threshold for topological subsystem color codes under very general external noise conditions. By transforming the problem into a classical disordered spin model, we estimate using Monte Carlo simulations that topological subsystem codes have an optimal error tolerance of 5.5(2)%. This means there is ample space for improvement in existing error-correcting algorithms that typically find a threshold of approximately 2%.

PACS numbers: 03.67.Pp, 75.40.Mg, 75.10.Nr, 03.67.Lx

Quantum computing promises to fundamentally further the bounds of computability, particularly in such fields as complexity theory and cryptography, and, in particular, the simulation of chemical and physical systems. Unfortunately, implementations of quantum computing proposals require precise manipulations of quantum systems which are highly susceptible to external noise. The technical feasibility of any quantum computer design thus heavily relies on efficient quantum error detection and recovery. This can be achieved, for example, by redundantly encoding quantum information in a code subspace of many physical qubits [1–3]. Such a suitable subspace is defined in terms of stabilizer operators [4, 5]—products of individual Pauli operators—and their corresponding eigenvalues.

Because stabilizers need to be measured during the error recovery procedure, geometric locality of the involved qubits is essential for practicality. Topological error correcting codes [6–11] achieve this by arranging qubits on a topologically nontrivial manifold with stabilizers acting only on neighboring qubits. These codes promise a reliable approach to quantum computing, because of their stability to errors [12–18]: A sizable fraction of physical qubits needs to fail before the logical information encoded in the system is lost beyond error correction.

To determine the error stability of topologically protected quantum computing proposals it is customary to map the error correction procedure onto the thermodynamic behavior of a disordered classical (statistical-mechanical) spin system [12, 14, 19]. There is a fruitful synergy between quantum computation and statistical mechanics: On the one hand, the stability of quantum computing proposals can be studied with the well-established machinery from statistical physics of complex systems, and on the other hand, it also opens the door to exotic applications of statistical models.

Unfortunately, there is one caveat: The stabilizers for surface codes (such as the Kitaev code [6]) and topological color codes [7] involve multiple qubits—four in the case of the Ki-

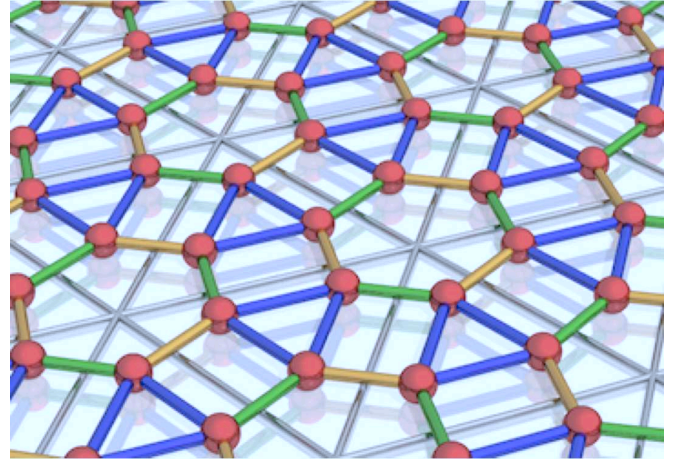


FIG. 1: (Color online) Graphical representation of the qubit arrangement for topological subsystem color codes on a regular triangular lattice. Each of the triangular unit cells (large gray triangles) contains three physical qubits (red balls). The two-qubit gauge generators $\sigma^w \otimes \sigma^w$ are shown in green ($w = x$), yellow ($w = y$) and blue ($w = z$). These are the lines connecting the qubits (red balls). They are arranged such that each physical qubit has two generators of z type, one of x type and one of y type. See main text for details.

taev code, six or eight for color codes. This immensely complicates physical realizations. However, in stabilizer subsystem codes [20, 21] some of the encoded logical qubits are “gauge qubits” where no information is encoded. This provides ancilla qubits to absorb decoherence effects and, in particular, allows breaking up the required measurements for error recovery into several individual measurement that involve a smaller number of qubits [20, 21], e.g., two. Hence, physical realizations are more feasible at the price of requiring additional qubits. Note that extensions and variants have also been proposed [22, 23].

A true advantage is given by *topological* subsystem codes [9] which combine the robustness of topologically based im-

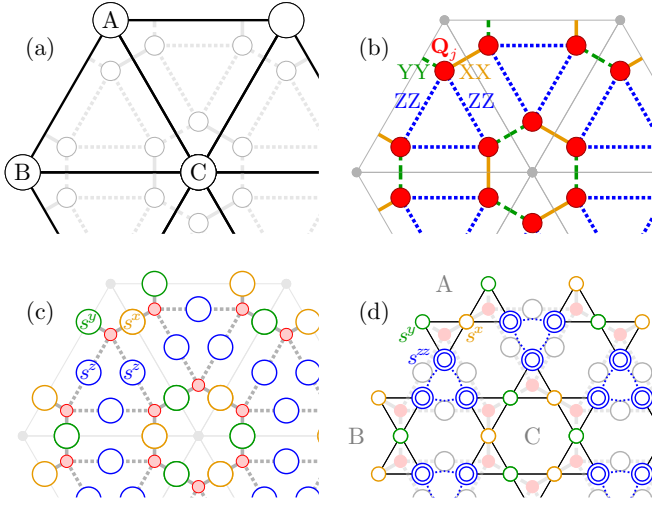


FIG. 2: (Color online) (a) A regular triangular lattice satisfies the vertex three-colorability requirement (indicated by A, B, C). (b) To construct a topological subsystem code, we place three qubits (red balls) inside each of the triangular unit cells and connect them with $\sigma^z \otimes \sigma^z$ gauge generators (dotted blue lines). The links between these triangles are assigned $\sigma^x \otimes \sigma^x$ and $\sigma^y \otimes \sigma^y$ gauge generators (yellow and green solid lines, respectively). (c) For the mapping, gauge generators represented by colored lines in (b) are associated with Ising spins $s^{x,y,z}$ and the qubits with interactions. (d) Introducing new Ising spin variables $s^{zz} = s^z s'^z$ allows for the removal of local \mathbb{Z}_2 symmetries.

plementations with the simplicity of subsystem codes where only measurements of neighboring qubits are required for recovery. As in the case of surface and color codes, the ideal error stability for topological subsystem codes can be computed by mapping the error recovery problem onto a classical statistical-mechanical Ising spin system where the disorder corresponds to faulty physical qubits. Here, using large-scale Monte Carlo simulations we compute the ideal error correction threshold for topological subsystem color codes affected by depolarizing noise. Our results show error correction is feasible up to 5.5(2)% faulty physical qubits. Remarkably, existing error correcting algorithms only reach a threshold of approximately 2% [24, 25], leaving ample room for improvement.

Topological subsystem codes and mapping.— A stabilizer subsystem code is defined by its gauge group \mathcal{G} . Its elements are Pauli operators that, by definition, do not affect encoded states. Namely, two states ρ and ρ' are equivalent if $\rho = \sum_i g_i \rho g_i'$ with g_i and g_i' elements in the algebra generated by \mathcal{G} .

Topological subsystem color codes [9] are constructed by starting from a two-dimensional lattice with triangular faces and three-colorable vertices. Here we consider the triangular lattice shown in Figs. 1 and 2(a). As indicated in Figs. 1 and 2(b), there are three physical qubits per triangle and the gauge group has 2-local generators G_i of the form $\sigma^w \otimes \sigma^w$, where $w = x, y$, and z .

Any family of topological codes shows a finite threshold for

a given local noise source. In other words, when the intensity of the noise is below the threshold, we can correct errors with any desired accuracy at the price of choosing a large enough code in the family. We are interested in the error threshold of topological subsystem codes under the effects of depolarizing noise, where each qubit is affected by a channel of the form

$$\mathcal{D}_p(\rho) = (1-p)\rho + \frac{p}{3} \sum_{w=x,y,z} \sigma^w \rho \sigma^w. \quad (1)$$

Here ρ represents the density matrix describing the quantum state of the qubit and $p \in [0, 1]$ its the probability for an error to occur. The depolarizing channel plays a fundamental role in quantum information protocols where the effects of noise need to be considered, e.g., in quantum cryptography [26, 27], quantum distillation of entanglement [28], and quantum teleportation [29].

It is expected that there exists a threshold value $p = p_c$ such that in the limit of large codes, for $p < p_c$ error correction succeeds with probability 1 and for $p > p_c$ the result is entirely random. Remarkably, for topological codes in general, one can relate p_c to a phase transition in a suitably-chosen classical disordered Ising spin model, as we detail next.

To construct the related classical statistical-mechanical system, we place an Ising spin $s_i = \pm 1$ for each gauge generator G_i . Single qubit Pauli operators σ^w are mapped onto interaction terms according to the generators G_i with which they do not commute, giving rise to a Hamiltonian of the general form

$$\mathcal{H}_\tau(s) := -J \sum_j \sum_{w=x,y,z} \tau_j^w \prod_i s_i^{g_{ij}^w}. \quad (2)$$

Here i enumerates all Ising spins and j all physical qubit sites, respectively. For each spin s_i the exponent $g_{ij}^w \in \{0, 1\}$ is 0 [1] if σ_j^w [anti]commutes with G_i . The signs of the couplings $\tau_j^w = \pm 1$ are then quenched random variables satisfying the constraint $\tau_j^x \tau_j^y \tau_j^z = 1$. For each j , they are all positive with probability $1-p$ and the other three configurations have probability $p/3$ each.

In our specific case the Hamiltonian has the geometry depicted in Fig. 2(c) and thus takes the form

$$\mathcal{H} = -J \sum_j^n (\tau_j^x s_j^y + \tau_j^y s_j^x) s_j^z \bar{s}_j^z + \tau_j^z s_j^x s_j^y, \quad (3)$$

where j enumerates qubit sites and spins are labeled, for each j , as shown in Fig. 2. Notice that z -labeled spins are arranged in triangles, and that flipping each of these triads of spins together does not change the energy of the system. Therefore, there is a \mathbb{Z}_2 gauge symmetry. We fix the \mathbb{Z}_2 gauge symmetry and at the same time simplify the Hamiltonian by introducing new Ising variables $s_j^{zz} = s_j^z \bar{s}_j^z$. Notice that these spins are constrained: If j, k, l are three-qubit sites in a triangle, $s_j^{zz} s_k^{zz} s_l^{zz} = 1$. The simulated Hamiltonian therefore reads [30]

$$\mathcal{H} = -J \sum_j^n \tau_j^x s_j^x s_j^{zz} + \tau_j^y s_j^y s_j^{zz} + \tau_j^z s_j^x s_j^y. \quad (4)$$

Note that the Hamiltonian in Eq. (4) has no local symmetries, but a global $\mathbb{Z}_2 \times \mathbb{Z}_2$ symmetry. Indeed, we can color spins according to their nearest colored vertex in the original lattice [Fig. 2(a)], producing three sublattices A, B, and C. Flipping the spins of two of these sublattices together leaves the energy invariant, giving rise to the indicated symmetry.

We are thus left with a random spin system with two parameters, T and p . It is expected that for low T and p the system will be magnetically ordered. In the ground states each sublattice has aligned spins and thus the sublattice magnetization is a good order parameter:

$$m = \frac{1}{N_{\mathcal{P}}} \sum_{i \in \mathcal{P}} s_i, \quad (5)$$

where $N_{\mathcal{P}} = L^2/3$ (L the linear system size) represents the number of spins in one of the sublattices. The threshold p_c for topological subsystem codes is recovered as the critical p along the Nishimori line [31]

$$4\beta J = \ln \frac{1-p}{p/3} \quad (6)$$

where the ferromagnetic phase of a sublattice is lost [12].

Numerical details.— We investigate the critical behavior of the classical Ising spin model [Eq. (4)] via large-scale parallel tempering Monte Carlo simulations [32, 33]. Both spin states and interaction terms are bit encoded to allow for efficient local updates via bit masking. Detecting the transition temperature $T_c(p)$ for different fixed amounts of disorder allows us to pinpoint the phase boundary in the p – T phase diagram (Fig. 4).

We choose periodic boundary conditions keeping in mind the colorability requirements. Then we can use the magnetization defined in Eq. (5) to construct the wave-vector-dependent magnetic susceptibility

$$\chi_m(\mathbf{k}) = \frac{1}{N_{\mathcal{P}}} \left\langle \left(\sum_{i \in \mathcal{P}} S_i e^{i\mathbf{k} \cdot \mathbf{R}_i} \right)^2 \right\rangle_T, \quad (7)$$

where $\langle \cdots \rangle_T$ denotes a thermal average and \mathbf{R}_i is the spatial location of the spin s_i . From Eq. (7) we construct the two-point finite-size correlation function,

$$\xi_L = \frac{1}{2 \sin(k_{\min}/2)} \sqrt{\frac{[\chi_m(\mathbf{0})]_{\text{av}}}{[\chi_m(\mathbf{k}_{\min})]_{\text{av}}} - 1}, \quad (8)$$

where $[\cdots]_{\text{av}}$ denotes an average over disorder and $\mathbf{k}_{\min} = (2\pi/L, 0)$ is the smallest non-zero wave vector. Near the transition ξ_L is expected to scale as

$$\xi_L/L \sim \tilde{X}[L^{1/\nu}(T - T_c)], \quad (9)$$

where \tilde{X} is a dimensionless scaling function. Because at the transition temperature $T = T_c$, the argument of Eq. (9) is zero (up to scaling corrections) and hence independent of L , we expect lines of different system sizes to cross at this point. If,

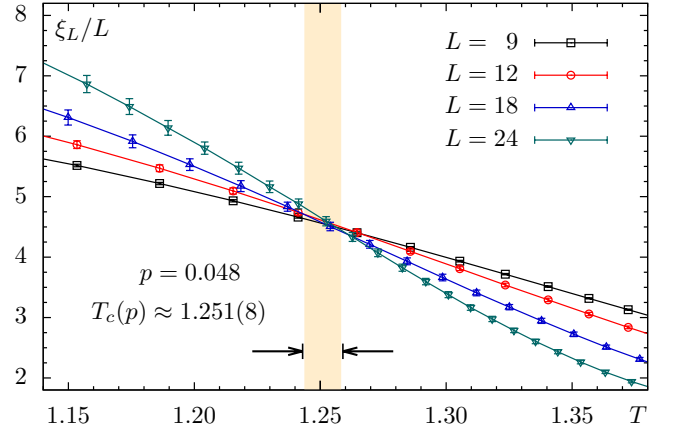


FIG. 3: (Color online) Crossing of the correlation function ξ_L/L with a disorder rate of $p = 0.048$. The data exhibit a clear crossing at a transition temperature of $T_c(p) \approx 1.251(8)$ [30]. The shaded area corresponds to the error bar in the estimate of $T_c(p)$. Note that error bars are calculated using a bootstrap analysis of 500 resamplings. Corrections to scaling are minimal at this disorder rate, but increase closer to the error threshold.

TABLE I: Simulation parameters: p is the error rate for the depolarizing channel, L is the linear system size, N_{sa} is the number of disorder samples, $t_{\text{eq}} = 2^b$ is the number of equilibration sweeps, T_{\min} [T_{\max}] is the lowest [highest] temperature, and N_T the number of temperatures used.

p	L	N_{sa}	b	T_{\min}	T_{\max}	N_T
0.000 – 0.020	9, 12	3 200	17	1.40	2.50	24
0.000 – 0.020	18	1 600	18	1.40	2.50	24
0.000 – 0.020	24	400	19	1.40	2.50	28
0.030 – 0.040	9, 12	4 800	18	1.25	2.40	28
0.030 – 0.040	18	2 400	19	1.25	2.40	28
0.030 – 0.040	24	800	20	1.25	2.40	32
0.045 – 0.060	9, 12	9 600	19	0.9	2.20	32
0.045 – 0.060	18	4 800	21	0.9	2.20	36
0.045 – 0.060	24	2 400	24	0.9	2.20	48

however, the lines do not meet, we know that no transition occurs in the studied temperature range.

When determining the transition temperature $T_c(p)$ for a given disorder rate p , the correlation functions ξ_L/L are obtained by averaging over several disorder realizations (governed by p) for every system size L . Because we are only able to investigate limited system sizes $L < \infty$, a careful analysis of finite-size effects is required when estimating the transition temperature in the thermodynamic limit.

In all simulations, equilibration is tested using a base-2 logarithmic binning of the data: Once the data for all observables agree for three logarithmically sized bins within error bars we deem the Monte Carlo simulation for that system size to be in thermal equilibrium. The simulation parameters can be found in Table I.

Results.— For the pure system ($p = 0$) there is a sharp transition visible directly in the sublattice magnetization. The transition temperature $T_{c,\text{pure}} \approx 1.65(1)$ has not been com-

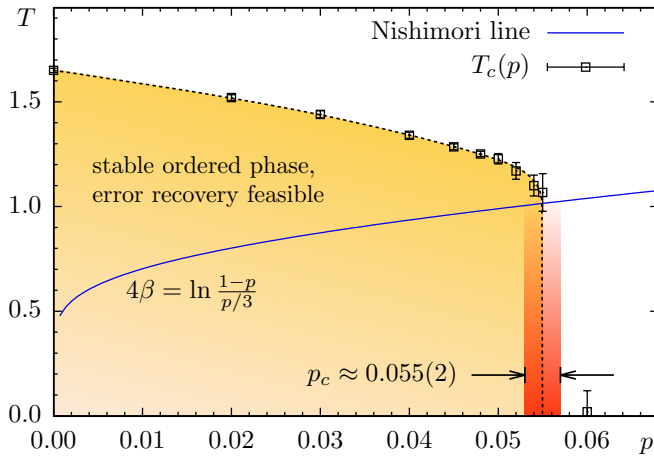


FIG. 4: (Color online) Computed phase diagram for the classical disordered spin model shown in Eq. (3). Each data point $T_c(p)$ on the phase boundary (dashed curve separating white and shaded regions) is calculated by locating the crossing in correlation function ξ_L/L for different system sizes L at a fixed disorder rate p . The Nishimori line (blue solid line) indicates where the requirement for the mapping [Eq. (6)] holds. The error threshold $p_c \approx 0.055(2)$ is found where the Nishimori line intersects the phase boundary between the ordered phase (shaded) and the disordered phase (not shaded, larger T and p). Below $p_c \approx 0.055(2)$ error correction is feasible. The (red) shaded vertical bar corresponds to the statistical error estimate for p_c .

puted before. For larger amounts of disorder, a possible transition can be located precisely by means of the two-point finite-size correlation function [Eq. (8)]. Sample data for a disorder strength of $p = 0.048$ (i.e., this would mean that on average 4.8% of the physical qubits have failed) are shown in Fig. 3, indicating a transition temperature of $T_c(p) = 1.251(8)$. At $p = 0.055(2)$, the lines only touch marginally such that both the scenario of a crossing as well as no transition are compatible within error bars. For error rates $p > p_c$, the lines do not meet, indicating that there is no transition in the temperature range studied.

The crossing of the critical phase boundary $T_c(p)$ with the Nishimori line [Eq. (6)] determines the error threshold to depolarization. Our (conservative) estimate is $p_c \approx 0.055(2)$. Our results are summarized in Fig. 4, which shows the estimated phase diagram.

Summary.— We have calculated numerically the error resilience of topological subsystem codes to the depolarizing channel by mapping the error correction procedure onto a statistical-mechanical Ising spin model with disorder. The large critical error rate of $p_c = 5.5(2)\%$, combined with a streamlined error recovery procedure that requires only two-qubit interactions, constitutes a promising implementation concept for quantum computing.

Acknowledgments.— M.A.M.-D. and H.B. thank the Spanish MICINN Grant No. FIS2009-10061, CAM research consortium QUITEMAD S2009-ESP-1594, European Commission PICC: FP7 2007-2013, Grant No. 249958, and UCM-BS Grant No. GICC-910758. Work at the Perimeter Institute

is supported by Industry Canada and Ontario MRI. H.G.K. acknowledges support from the SNF (Grant No. PP002-114713) and the NSF (Grant No. DMR-1151387). We thank ETH Zurich for CPU time on the Brutus cluster and the Centro de Supercomputación y Visualización de Madrid (CeSViMa) for access to the Magerit-2 cluster.

-
- [1] P. W. Shor, Phys. Rev. A **52**, R2493 (1995).
 - [2] A. M. Steane, Phys. Rev. Lett. **77**, 793 (1996).
 - [3] E. Knill and R. Laflamme, **55**, 900 (1997), Phys. Rev. A.
 - [4] D. Gottesman, Phys. Rev. A **54**, 1862 (1996).
 - [5] A. R. Calderbank and P. W. Shor, Phys. Rev. A **54**, 1098 (1996).
 - [6] A. Y. Kitaev, Ann. Phys. **303**, 2 (2003).
 - [7] H. Bombin and M. A. Martin-Delgado, Phys. Rev. Lett. **97**, 180501 (2006).
 - [8] H. Bombin and M. A. Martin-Delgado, Phys. Rev. B **75**, 075103 (2007).
 - [9] H. Bombin, Phys. Rev. A **81**, 032301 (2010).
 - [10] S. Bravyi, B. M. Terhal, and B. Leemhuis, New J. Phys. **12**, 083039 (2010).
 - [11] J. Haah, Phys. Rev. A **83**, 042330 (2011).
 - [12] E. Dennis, A. Kitaev, A. Landahl, and J. Preskill, J. Math. Phys. **43**, 4452 (2002).
 - [13] R. Raussendorf and J. Harrington, Phys. Rev. Lett. **98**, 190504 (2007).
 - [14] H. G. Katzgraber, H. Bombin, and M. A. Martin-Delgado, Phys. Rev. Lett. **103**, 090501 (2009).
 - [15] S. D. Barrett and T. M. Stace, Phys. Rev. Lett. **105**, 200502 (2010).
 - [16] G. Duclos-Cianci and D. Poulin, Phys. Rev. Lett. **104**, 050504 (2010).
 - [17] D. S. Wang, A. G. Fowler, and L. C. L. Hollenberg, Phys. Rev. A **83**, 020302 (2011).
 - [18] A. Landahl, J. T. Anderson, and P. Rice, (arXiv:quant-ph/1108.5738) (2011).
 - [19] C. Wang, J. Harrington, and J. Preskill, Ann. Phys. **303**, 31 (2003).
 - [20] D. Poulin, Phys. Rev. Lett. **95**, 230504 (2005).
 - [21] D. Bacon, Phys. Rev. A **73**, 012340 (2006).
 - [22] S. Bravyi, Phys. Rev. A **83**, 012320 (2011).
 - [23] G. M. Crosswhite and D. Bacon, Phys. Rev. A **83**, 022307 (2011).
 - [24] H. Bombin, G. Duclos-Cianci, and D. Poulin (2011), (arXiv:quant-ph/1103.4606).
 - [25] M. Suchara, S. Bravyi, and B. Terhal, J. Phys. A **44**, 155301 (2011).
 - [26] P. W. Shor and J. Preskill, Phys. Rev. Lett. **85**, 441 (2000).
 - [27] B. Kraus, N. Gisin, and R. Renner, Phys. Rev. Lett. **95**, 080501 (2005).
 - [28] C. H. Bennett, G. Brassard, S. Popescu, B. Schumacher, J. A. Smolin, and W. K. Wootters, Phys. Rev. Lett. **76**, 722 (1996).
 - [29] G. Bowen and S. Bose, Phys. Rev. Lett. **87**, 267901 (2001).
 - [30] In the simulations we set the energy scale $J = 1$, i.e., all temperatures and estimates of T_c are dimensionless.
 - [31] H. Nishimori, Prog. Theor. Phys. **66**, 1169 (1981).
 - [32] K. Hukushima and K. Nemoto, J. Phys. Soc. Jpn. **65**, 1604 (1996).
 - [33] H. G. Katzgraber, S. Trebst, D. A. Huse, and M. Troyer, J. Stat. Mech. P03018 (2006).